WILEY-VCH

DOI: 10.1002/ ((please add manuscript number))
Article type: (Full paper)

Blue and deep-blue emitting organic lasers with top-layer distributed feedback resonators

*Victor Bonal, Jose M. Villalvilla, Jose A. Quintana, Pedro G. Boj, Naiti Lin, Shoya Watanabe, Karolis Kazlauskas, Ona Adomeniene, Saulius Jursenas, Hayato Tsuji, Eiichi Nakamura, María A. Díaz-García**

V. Bonal, Dr. J.M. Villalvilla, Prof. M.A. Díaz-García
Dpto. Física Aplicada and Instituto Universitario de Materiales de Alicante (IUMA), Universidad de Alicante; Alicante 03080; Spain.
E-mail: maria.diaz@ua.es

Dr. J.A. Quintana, Dr. P.G. Boj
Dpto. Óptica, Farmacología y Anatomía and IUMA, Universidad de Alicante, Alicante 03080, Spain

Dr. Naiti Lin, Prof. E. Nakamura
Department of Chemistry, School of Science, The University of Tokyo, Hongo, Bunkyo-ku, Tokyo 113-0033; Japan.

Shoya Watanabe, Prof. H. Tsuji
Department of Chemistry, Faculty of Science, Kanagawa University, 2946 Tsuchiya, Hiratsuka 259-1293; Japan.

Dr. K. Kazlauskas, Dr. Ona Adomeniene, Prof. S. Jursenas
Institute of Photonics and Nanotechnology, Vilnius University, Saulėtekio av. 3, LT-10257 Vilnius, Lithuania

Keywords: organic lasers, solution-processed, distributed feedback lasers, polymeric resonators

Abstract

All-solution processed surface-emitting organic distributed feedback (DFB) lasers are attractive devices for low-cost applications. Here, we report lasers emitting in the spectral region between 375 and 475 nm in which both, active material and resonator (one dimensional relief gratings) are based on solution-processable polymer films. Ten different organic compounds dispersed in polystyrene are used as active layers of the prepared devices. They include various Carbon-bridged oligo(*p*-phenylenevinylene) (COPV*n*, with *n* = 1,2) derivatives, and two terfluorene compounds. The synthesis and complete optical and amplified spontaneous emission properties of one of the COPV1 compounds, COPV1(Me)-*t*-

Bu, designed for deep-blue emission, is also included. The feasibility of the resonator fabrication, performed by holographic lithography with a dichromated gelatine photoresist over the active film, is successfully demonstrated for all devices. Remarkably, no resolution limitations are found even for the lowest grating period (235 nm) required for the fabrication of the laser based on COPV1(Me)-*t*-Bu. It is also demonstrated that the rectangular grating profile with duty cycle 0.75:0.25 (hill:valley), is very convenient to optimize the resonator efficacy.

1. Introduction

Lasers based on organic active media have attracted great attention for many years, mainly because they enable wavelength tuning across the visible spectrum.[1,2] In the last two decades, there has been a major focus on thin-film organic lasers (TFOLs), motivated by various advantages in comparison to other types of organic lasers, such as monolithic-based solid-state dye lasers or commercially available liquid dye lasers.[1–4] TFOLs are compact, can be mechanically flexible and be prepared in a low-cost manner, and can be pumped with low-power sources, in some cases even with diode lasers or light emitting diodes. Moreover, advances towards electrically-pumped TFOLs have been recently reported.[5] On the other hand, conventional solid-state or liquid dye lasers have large sizes and require very powerful laser sources to operate. The distributed feedback (DFB) laser, consisting of an organic waveguide active film and a relief diffractive grating as laser resonator, has been one of the most widely investigated TFOLs. In particular, DFB lasers with gratings operating in the second-order of diffraction are attractive for certain applications, such as sensing,[6–8] because the emission is perpendicular to the surface film and can be single mode.[1–3]

With major advances achieved in the preparation of organic DFB lasers, mainly focused on reducing the laser threshold (minimum pump energy required to operate), many recent efforts are focusing on all-solution processed devices, that is, with both, active film and laser resonator made of organic material.[9–11] Such all-solution processed devices would truly exploit the pursued advantages of TFOLs of low cost and mechanical flexibility. Noticeably, while best performing DFBs reported in the literature have high-quality gratings engraved on inorganic substrates by expensive methods, such as electron-beam lithography, lasers based on solution-processed resonators have generally a more limited threshold performance.[1–3,9–11]

In this context, an important recent achievement was the demonstration of a very successful all-solution processed organic DFB laser, based on a top-layer solution processed

dichromated gelatin (DCG) polymeric resonator.[12] These devices showed low thresholds and long operational stabilities, comparable to those of devices with standard gratings engraved on inorganic substrates, and superior laser efficiencies. Additionally, they allowed wavelength tunability within the same chip.

So far, all the reported top-layer DCG resonator lasers, emit in the green and red part of the optical spectrum.[12,13] Thus, the fabrication of top-layer polymeric resonator devices operating in the blue and deep-blue regions remains as a challenge, firstly because of possible resolution limitations in the resonator fabrication, imposed by the relatively low grating periods required, and secondly, because of the need of efficient laser dyes operating in those regions.[14]

With regards to the active laser material, among a wide variety of materials used, carbon-bridged oligo(*p*-phenylenevinylene)s (COPV*n*, with *n* = 1–6), dispersed in polystyrene (PS), used as passive matrix, have demonstrated a great success to be used for DFB lasers because of the rigid planar molecular structure that is advantageous to enhance emission efficiency.[15–17] These compounds emit at wavelengths that cover a wide range of the visible spectrum (380–600 nm), where emissions in the blue side correspond to the shorter COPV*n*, with *n* = 1 and 2. In the first lasing studies on these materials, the performance of these blue-emitting dyes was inferior than that of longer COPV*n* compounds (COPV3-6),[15] as a consequence of their lower photostability. Such limitations have been recently overcome through two different synthetic strategies, both aiming to protect the molecular terminal site that is labile to photodegradation: a homopolymer of COPV1,[18] and sterically protected COPV*n* derivatives with bulky substituents on the terminal sites.[19] The homopolymer, however, emits green because of the extension of conjugation, while the latter compounds show blue emission by taking advantage of their short conjugation lengths with improved photostability.

Here, we report deep-blue and blue emitting, top-layer polymeric resonator DFB lasers based on ten different compounds (see device scheme and chemical structures in **Figures 1a** and **1b**,

respectively). Prior to laser fabrication, the resolution of the process for making grating resonators with periods between 200 and 500 nm is analyzed. This range covers a broad range of lasers, from deep blue to the near IR region. In addition, it will be shown that other grating parameters, such as the type of grating profile and its duty cycle, have a great influence on the resonator efficacy. Once the feasibility of the resonator preparation process is demonstrated, we proceed to fabricate DFB lasers using as active films PS doped with one of the compounds shown in Figure 1b. These compounds include the recently synthesized COPV1 and COPV2 derivatives with sterically protecting groups on the terminal sites,[19] and two terfluorene compounds,[20] which emit in the spectral band between those of the COPV1 and COPV2 families. These systems show amplified spontaneous emission (ASE) in the range 385-465 nm. Additionally, the synthesis and complete optical and ASE characterization of a novel COPV1 compound, denoted as COPV1(Me)-*t*-Bu, that shows even shorter wavelengths in deep-blue region (maximum photoluminescence (PL) and amplified spontaneous emission (ASE) peaks at 376 nm), is reported here. For the set of devices prepared, the emission wavelength is finely tuned in a deep blue to blue range through the selection of the dyes among them and proper resonator design.

INSERT FIGURE 1

2. Results and discussion

The device structure of the top-layer polymeric resonator (Figure 1a) consists of an active film deposited over a fused silica (FS) substrate and a top-layer grating resonator. The active film of thickness *h* is based on PS doped with a small percentage of an organic laser dye. The resonator is a one-dimensional (1D) surface-relief grating, engraved by holographic lithography (HL) in a DCG photoresist layer, and it is characterized by a set of basic geometrical parameters: Λ, the grating period, *d*, the grating modulation depth, and *s*, the thickness of the residual photoresist layer. For all the lasers prepared in this work, there is no

residual layer (s = 0), because this is convenient to obtain the largest possible laser efficiencies.[13]

In a 1D DFB organic laser with such structure, the lasing wavelength is close to the so-called Bragg wavelength, λ_{Bragg}, given by [1,2]

$$\lambda_{Bragg} = 2n_{eff}\Lambda/m \quad (1)$$

where n_{eff} is the effective refractive index of the waveguide, which depends on *h*, as well as on the refractive indexes of the film, substrate and cover. All the DFB devices prepared in this work operate in the second order of diffraction, that is $m = 2$ in the Bragg condition. In this condition, the laser light is coupled out in a direction perpendicular to the film by first-order diffraction. Thus, the grating plays two roles: (i) it provides feedback for the light propagating along the film and (ii) it extracts the light out of the device. In order to obtain an optimized performance, it is important to have a fine control on the grating geometrical parameters. Particularly, the grating period, Λ, (typically below 500 nm for second-order DFBs based on dye-doped polymers) should be well defined. Besides, the grating modulation depth, *d*, must be lower than 200 nm to maintain external losses at a low level.[13]

2.1. Resonator fabrication: resolution and effect of the duty cycle

The second-order DFB lasers prepared in this work emit at wavelengths between 375 and 475 nm. Their fabrication required resonators with grating periods in the range 230-300 nm. For a given compound, Λ was chosen to obtain λ_{Bragg} (Equation 1) matching its PL spectrum. Since the dye percentage is small for COPV1 and COPV2 derivatives (between 2 and 7 wt%), the refractive index value of the active film can be assumed to be equal to that of an un-doped PS film. On the other hand, the refractive indices of F-hex and F-et active films with larger concentrations of dye (10 and 50 wt%, respectively) were calculated by a modification of the envelope method, applicable to very thin films.[21]

2.1.1. Resolution of the fabrication process

The resolution of the fabrication process to make gratings with Λ values between 200 and 500 nm (frequencies 5000-2000 mm^{-1}) has been investigated. This range includes the needs for lasers emitting from the deep-blue to the near IR. Such investigation has been carried out through a combination of diffraction efficiency measurements and modelling with the Gsolver software program[22] as described in detail below. Results are collected in **Figure 2.** It should be remarked that detailed resolution studies have not been previously performed for the resonator fabrication process and DCG photoresist used here. Special attention is devoted to the gratings with the smallest periods (used for deep-blue emitting lasers), because limitations might arise, as reported for other photoresists.[23]

Firstly, it should be noted that the low-limit of the range of explored Λ values, 200 nm, is established by the wavelength of the laser used in the HL grating recording process, $\lambda = 364$ nm. This is performed in a Lloyd's mirror interferometer configuration (see Scheme of the recording geometry in Figure S1, supporting information), for which the period Λ of the interference pattern is given by

$$\Lambda = \lambda/(2 \sin \delta) \qquad (2)$$

where δ is half of the interbeam angle. According to this, the smallest possible Λ is $\lambda/2$. Secondly, fabrication parameters have been adjusted to obtain gratings with optimized performance (i.e. with lowest possible threshold and highest laser efficiency, simultaneously), according to previous studies: initial thickness of the DCG layer, s_0 = 120 nm; average exposure E_{av} = 45 mJ cm^{-2}; and dry-development time to obtain $s \sim 0$, t_D = 10.5 min.[13] The E_{av} value is chosen to be close to saturation conditions at which diffraction efficiency no longer increases.[23]

After processing, diffraction efficiency, η, was measured for the various gratings prepared. Here, η corresponds to the ratio between the transmitted first-order diffracted and the incident light intensities (see scheme in Figure 2a). This method to obtain η follows a holographic criterion, based on illuminating all gratings with light of the same wavelength, polarization and incident angle (δ), such as those used in the recording process. This method is convenient here because it allows analysing gratings with very low grating periods, avoiding volume effects in the diffraction gratings. The measured η values for the various gratings, each with a different Λ, are shown in Figure 2b. A contour plot of simulated η as a function of Λ and the grating incident angle ω, performed by means of the Gsolver software program,[22] is shown in Figure S2 in supporting information. The particular values of this plot, which comply with Eq (2), have been represented in Figure 2b with a full line. A good agreement is found between experiments and simulations. Then, from the experimental η values of Figure 2b, the grating depth, *d*, for each grating was calculated using Gsolver (Figure S3 in supporting information). Results of *d* versus Λ are shown in Figure 2c. It is seen that the modulation transfer is independent of the period and the resulting *d* is 110±7 nm. This means that all these periods are well resolved with our HL process. It is also observed that the selectivity of the development process is approximately 10. A previous study using dichromated polyvinylalcohol (DCPVA) and a similar grating fabrication process, showed a light sensitivity five times higher than that of DCG, but a worse resolution since the modulation transfer decreased for periods lower than 300 nm.[23]

INSERT FIGURE 2

2.1.2. Effect of the duty cycle on the resonator performance

The HL fabrication parameters used to prepare the resonator determine the type of grating profile and its duty cycle, *D*, defined as the ratio between the grating ridge width, *L*, and the

period ($D = L/\Lambda$). For the gratings prepared in this work, the resulting profile is rectangular and D is in the range 0.75- 078. This is illustrated through the field emission scanning electron microscope (FESEM) images shown in **Figure 3**a and 3b. The reason for such a rectangular profile, far from the sinusoidal profile of the fringes of interference, is the use of a value of E_{av} close to saturation conditions. Besides, since the DCG is a negative resist, D is above 0.5.[24]

INSERT FIGURE 3

The influence of D on the resonator efficacy for its two functions (to provide feedback for in-plane propagation and to extract light out of the device) is analysed here considering the laser geometry scheme shown in Figure 3c. After excitation, the light emitted inside the active layer is diffracted by the grating in different directions, corresponding to the various orders of diffraction. The second-order diffracted beam (-2R), reflected in a direction opposite to that of the incident beam, provides the in-plane feedback. On the other hand, the first-order diffracted beam, in transmission and reflection (-1T and -1R, respectively), correspond to the light extracted out of the device. Finally, the beam 0R, reflected at an angle equal to the incident angle, transports most of the energy and propagates along the active layer at an angle greater than the limit angle. It is clear that the distribution of the energy among the various diffracted beams, which determines the efficacy of the in-plane feedback and light extraction functions, strongly depends on the grating profile and its D value.

Relationships between diffracted beams are usually considered through two amplitude coupling coefficients: κ_1, arising from the two first-order beams -1T and -1R, which describe losses, and therefore the light extraction; and κ_2, arising from the second-order beam -2R, which provides the in-plane feedback.[25] These coefficients can be calculated from the grating efficiencies at the corresponding order η_m, using the following phenomenological equation:[26–28]

$$\kappa_m = \eta_m^{1/2} B \quad (3)$$

Here, B represents the bounce rate, i.e., the number of bounces in the waveguide per unit length and is given by

$$B = \left(2h_{eff} \tan\theta\right)^{-1} \quad (4)$$

where it is assumed that the reflection angle θ is coincident with the bounce angle and h_{eff} is the effective waveguide thickness, i. e., the thickness of the active layer plus the penetration depth of the field in the diffraction grating and the adjacent layers (see Figure 3d). In fact, the light interaction with the grating takes place through the evanescent wave of the light travelling along the active film, but for the purpose of the present analysis an optics ray model is a good approximation.

Figure 3e shows calculations of the coupling coefficients κ_1 y κ_2 as a function of D for two of the fabricated lasers. Particularly, we have considered the device parameters for the lasers with the lowest and the highest grating periods, 235 and 300 nm, respectively. Diffraction efficiencies at θ angle were calculated with the Gsolver program, using the geometrical grating parameters and the ray geometry of the DFB laser shown in Figure 3c. The effective thickness of the waveguides were calculated following the procedure indicated by Luo et al.,[27] which stablishes an approximation valid for practical DFB laser structures. In this case, h_{eff} has been calculated by adding to the active film thickness (h) the contribution of the grating (weighted by the duty cycle) and the penetration depth in both, the substrate and the air. It can be seen in Figure 3e that the shape of the curves for both devices is similar. The coefficient κ_1, related to the amount of emitted laser light, is maximum for a D value of approximately 0.4; on the other hand, the coefficient κ_2, related to the feedback, presents local maxima for D values of approximately 0.25 and 0.85, and a minimum for $D \sim 0.45$. As indicated in Figure 3e through vertical dotted lines, the particular values of κ_1 and κ_2 for the real devices, whose $D = 0.77$, are around 230 and 350 cm^{-1}, respectively. These values

indicate that, according to this model, for these devices the losses are moderate and the feedback is near the maximum. So we can conclude that the process used for recording the gratings (designed to obtain an optimized laser performance), which produces a rectangular profile with $D \sim 0.75$, is appropriate to be used as resonators of these blue and deep-blue DFB lasers.

2.2. Active films: synthesis and optical characterization

2.2.1. Synthesis of active compounds

Compound COPV1(Me)-*t*-Bu was synthesized based on Friedel-Crafts reaction of COPV1(Me)[29] with *tert*-BuCl (Scheme S1 in supporting information; For details, see synthesis and spectral data of the new compound COPV1(Me)-*t*-Bu in the supporting information file). The synthesis of all the other compounds was done following methods previously reported.[15,19,20]

2.2.2. Optical characterization of active films without resonators

Active materials consisted of PS films, hosting one of the derivatives of Figure 1b, deposited on FS plates. The absorption (ABS), PL and ASE spectra of the film containing COPV1(Me)-*t*-Bu are shown in **Figure 4**a and a complete list of optical and ASE parameters is shown in Table S1 in the supporting information section. It should be remarked that COPV1(Me)-*t*-Bu has emissions in the deep-blue spectral region (i.e. maximum PL and ASE occur at 376 nm) with shortest PL and ASE wavelengths among the COPV1 compounds used in this work (see Figure 4a, inset). An additional feature for the COPV1(Me)-*t*-Bu film is that its absorption coefficient is around 3 times larger than that of the COPV1 derivative with aromatic substituents on the bridging carbon atoms, denoted as COPV1(Ar) in this paragraph to avoid confusion (see Table S1 in supporting information). This is because the COPV1(Ar)s show homoconjugation through the bridging carbon atoms,[30,31] which reduces the overlap between HOMO and LUMO to decrease the oscillator strength of the HOMO-LUMO transition,

whereas such effect is smaller for COPV1(Me) with lateral alkyl substituents to maintain relatively larger oscillator strength (Figure S4 in supporting information). This larger absorption might be the reason for its lower ASE threshold (750 μJ cm^{-2}), in comparison to COPV1(Ar) (900 μJ cm^{-2}). Interestingly, when comparisons are made taking the film absorbance at the excitation density into account, its threshold is similar to that of the COPV2 compounds (see Figure S5 in supporting information).

For the rest of the active compounds used, ASE occurs at longer wavelengths (spectra shown in Figure S6 in supporting information): the COPV2 family emits between 464 and 475 nm,[15,19] and the terfluorene compounds at around 420 nm,[20] which is located between the emission bands of COPV1 and COPV2 families (see **Table 1**). The terfluorene compounds are particularly interesting for their low ASE thresholds, although to date, no lasers based on them have been reported.

INSERT FIGURE 4

2.3. DFB fabrication and characterization

DFB lasers were fabricated by depositing DCG layers over the active films (optical properties discussed in Section 2.2.2.), and then recording gratings as described in Section 1. A wide set of devices, emitting across a wide spectral range (around 100 nm), between 375 and 475 nm, have been prepared using the various compounds. Their properties are analyzed through results shown in Figures 4b-e and Table 1. For a given compound, the grating period Λ was chosen to obtain lasing at a wavelength, λ_{DFB}, close to λ_{ASE}, at which gain is maximum. Spectra for a selection of ten devices, each containing a different compound, are shown in Figure 4b. Noticeably, we have a very fine design control over the desired λ_{DFB} value thanks to the versatility of the HL technique used to engrave the gratings. This is illustrated in Figure 4c, which shows the spectra for a set of COPV1(Me)-*t*-Bu lasers, all based on active films with the same dye content and film thickness (see details in Table S2 in supporting

information) and resonators of different Λ. It is seen that their emissions vary within a range of around 10 nm. Note that the threshold keeps at a low value, 1000 μJ cm^{-2}, for most of this range. This is because *h* (315 nm for the COPV1(Me)-*t*-Bu lasers) is uniform across the device due to its top-layer resonator configuration. It constitutes an advantage in comparison to other methods for wavelength tuning, such as the wedged configuration, in which the threshold varies considerably when changing λ_{DFB}.[32] Data for additional devices based on the other derivatives are provided in the supporting information section (Table S2). The emission linewidths of the reported laser spectra are limited by the spectral resolution of the spectrometer (1.3 nm, defined as the full width at half of the maximum). But according to higher-resolution measurements on red-emitting lasers, based on the same type of resonator and device architecture used here, they are expected to be < 0.13 nm.[11,12] For such spectral linewidths, the corresponding resonator quality factors, estimated for emission at λ ~ 400 nm, would be Q > 3000. This value is in accordance to values recently reported (Q = 1933) for other blue DFB lasers.[33]

All DFB lasers prepared emit linearly polarized light, in a direction parallel to the grating lines. This indicates that the laser mode is associated to the fundamental transverse electric waveguide mode TE_0. Figure 4d shows images of the light emitted by two of the lasers, based on COPV2-Tip and F-hex. The beam divergence observed in the direction perpendicular to the grating lines is ~ $5 \cdot 10^{-3}$ rad.

In terms of laser threshold, the performances of the terfluorene and COPV2 compounds are very good, with values of a few kW cm^{-2} (see Table 1). Threshold data are extracted from plots of the output intensity versus the pump energy density, E_{pump}, which show a drastic change of slope at the threshold, such as the one shown in Figure 4d for the devices based on COPV2-Tip and F-hex. The threshold values, which can also be extracted from the change in the emission linewidth (Figure S7 in supporting information), are comparable to those of

state-of-the-art DFB lasers based on PDI[34] and COPV3-6[15]. Evidence of lasing is also illustrated through Figure 4e, which displays the evolution of the emission spectrum as E_{pump} is increased. At a low E_{pump} value (i.e. below the threshold), a characteristic Bragg dip that corresponds to λ_{Bragg} in Eq. 1, is observed. As E_{pump} increases, a narrow lasing peak raises at a wavelength a few nm above this value. This is in accordance with predictions of coupled mode theory for devices with pure index coupling, such as the top-layer DFB lasers used in this work.[25,35,36] It is interesting to discuss the relation of the obtained DFB thresholds with the ASE threshold of the corresponding films (see Tables 1 and S2 and Figure S5). Although the DFB and the ASE thresholds are different quantities and cannot be directly compared (the type of sample and the pumping and collection geometries are different, as well as the amplification mechanisms involved), from previous experience with many different materials, the DFB thresholds are generally somewhat below the ASE threshold (by around two times, for optimized lasers based on dye-doped polymers and 1D DFB resonators). This is generally the case for the COPV2 compounds (for example, for COPV2-Tip, $E_{th\text{-}DFB}$ = 20 μJ cm^{-2} and $E_{th\text{-}ASE}$ = 40 μJ); but not for the COPV1 ones, for which the DFB threshold is slightly larger than the ASE threshold (for example, for COPV1(Me)-*t*-Bu, $E_{th\text{-}DFB}$ = 1000 μJ cm^{-2} and $E_{th\text{-}ASE}$ = 750 μJ cm^{-2}). Taking into account that the COPV1 compounds absorb precisely at the wavelength of the Argon laser used in the holographic recording process (λ = 364 nm), we considered that these differences might be due to film damage during grating recording. In order to clarify this, we performed some additional experiments on films without resonators, selecting one compound for each class of materials, particularly COPV1-t-Bu(Me) and COPV2. Thus, we recorded the ABS and PL spectra and measured the PLQY (photoluminescence quantum yield) and the ASE threshold for the films, before and after illumination with the Argon laser (λ = 364 nm) used for grating fabrication. In a second experiment, the possibility of damage due to exposure to an oxygen plasma (under conditions

similar to those used during the grating development process), was also investigated in the films, again by recording the ABS, PL, PLQY and ASE threshold before and after exposure. For both experiments, similar results were obtained before and after illumination and oxygen exposure, respectively (more details in Supporting information). So, it can be concluded that, within experimental error, the light and oxygen exposure of the films during the grating fabrication process do not seem to negatively affect their optical properties. So, they are not the reason for the larger-than-expected DFB thresholds observed for the COPV1 materials. Further studies to clarify this will be needed in the future.

With regards to the operational lifetime of the prepared lasers, it is reasonably good for devices based on F-hex and COPV2-Tip, with values of 1.2×10^4 and 7.7×10^4 pump pulses, under excitation two times above threshold. Although these values are inferior in comparison to red-emitting devices based on COPV6, it is remarkable the significant improvement observed in the device based on COPV2-Tip in comparison to that of COPV2. This is a consequence of the presence of Tip groups at the COPV2 terminal positions, which provide kinetic protection against molecular photoreaction.[19]

Finally, it is useful to compare the performance of the DFB lasers prepared here to state-of-the-art DFB lasers based on solution-processed active films and emitting in the same spectral range. A selection of such lasers, with their corresponding parameters, are listed in Table S3 in supporting information. There is a variety of systems emitting in the range 430-470 nm (as the COPV2 compounds) based on small molecules,[37,38] dendritic starbursts[39] and conjugated polymers.[40,41] Less devices have been reported with emissions in the deep blue (362-394 nm)[42] (as the COPV1 derivatives). Some of them have shown very low thresholds (< 0.1 kW cm^{-2}),[39,40] but in those cases the DFB gratings are engraved on inorganic substrates. Note that lasers with the gratings engraved on polymeric layers (such as the ones used in our devices), or directly on the active films, are usually larger (see for example data for PFO in Table S3).[41] On the other hand, it should also be remarked, that in most of these

low-threshold lasers, the active materials are neat films, as opposed to the dye-doped films used in our devices. Thus, film absorption is typically two orders of magnitude larger for the neat films (see data for PFO[40] in Table S3). This explains their generally lower ASE thresholds (and therefore DFB thresholds) in comparison to dye-doped materials. Nevertheless, an advantage of diluting in a matrix (despite the larger thresholds) is that operational lifetimes are generally longer. So, these materials offer a way to simultaneously optimize both parameters (threshold and lifetime).[15] With regards to the wavelength tunability for a given compound, it is generally obtained by either changing the grating period or film thickness, but this influences the threshold. At this respect, a distinctive feature of the top-layer resonators used in our devices is that gratings of various periods can be engraved over the same active film (of uniform thickness). Thus, wavelength tunability can be achieved within the same chip while preserving the threshold.[12]

3. Conclusions

A series of blue and deep-blue-emitting hydrocarbon materials have been examined to fabricate all-solution processed organic DFB lasers: two terfluorene compounds, and various carbon-bridged oligo(p-phenylenevinylene) (COPV*n*, with n = 1 and 2) derivatives. Furthermore, a new derivative, COPV1(Me)-*t*-Bu, has been synthetized to find that it presents deep-blue emission and better optical performance such as a higher absorptivity.

Rectangular DCG gratings with duty-cycle 0.75 have been recorded to be used as top resonators. No resolution limitations were found even for the lowest period required for deep-blue emission. In addition, this grating profile was proven to be very convenient to optimize the resonator efficacy providing feedback and extracting light out of the device. Noticeably, a very fine design control over the desired λ_{DFB} value was possible thanks to the versatility of the HL technique used to engrave the gratings.

The fabricated devices present improved laser properties compared to the previously reported DFB lasers with inorganic gratings. In terms of laser threshold, the performances of the

terfluorene and COPV2 compounds are very good in the context of lasers based on dye-doped polymers as active film, with values of a few kW cm^{-2}. With respect to the operational lifetime, that of the device based on COPV2-Tip is reasonably good in comparison to that of COPV2. This is a consequence of the presence of Tip groups at the terminal positions of COPV2, which provide kinetic protection against photoreaction.

Overall, this work has demonstrated the successful use of top-layer DCG gratings as resonators for blue-emitting DFB lasers. The devices prepared for that purpose consisted of dyes dispersed in polymers, but many other types of active materials could be used. Thus, this type of resonators have great potential for the development of high performing all-plastic DFB laser devices.

4. Experimental Section

Thin film and resonator fabrication

Thin films based on PS (Sigma Aldrich, M_w = 35000 g/mol) doped with different materials (between 2 and 7 wt% for COPV1 and COPV2 derivatives, 10 wt% for F-hex and 50 wt% for F-et) were spin coated at 3000 rpm on FS substrates (25 × 25 × 1 mm) using toluene as solvent. For COPV1 and COPV2, we chose concentrations that provide ASE with simulatneously optimized threshold and photostability.[15] Then, within each series of these two compounds, we have used the same dye concentration in the films, expressed in moles of dye per gram of PS (see Table S2). Such selection enabled proper analysis of the effect of the substituents on the dye ASE behaviour.[19] For F-ex and F-hex, the concentrations (in wt%) used are those that provided the lowest ASE thresholds according to previous optimization studies.[20] Film thickness (values for all the devices prepared are listed in Table S2) was determined from the transmission spectrum using a modification of the envelope method.[21] The percentage of PS in the solvent was adjusted between 4 and 9 wt% to obtain proper thickness for the films, so they constituted waveguides supporting only fundamental

transversal modes with a high confinement factor ($\Gamma \approx 90\%$). This helps to minimize losses, and thus to optimize the ASE performance.[43,44]

The first step in the resonator fabrication is the deposition of a DCG film by spin coating from a water solution. The concentrations of gelatine (Russelot, 200 bloom) and ammonium dichromate, used as sensitizer, were 2.2 wt% (with respect to water) and 35 wt% (with respect to gelatine), respectively. After the film deposition, one-dimensional gratings were recorded by HL using the Lloyd configuration (Figure S1) with light from an Ar laser emitting at 364 nm and an average exposure of 45 $\mu J\ cm^{-2}$. The next step consisted on desensitizing the DCG layers in a cold water bath (15 ^{o}C). Lastly, surface-relief gratings were obtained by dry development in an oxygen plasma using a surface treatment machine Diener Zepto.[12,13] All resonators had a grating depth of ~110 nm and were fabricated on FS substrates to characterize the gratings or on active films to build DFB laser devices.

The grating depth was calculated by measuring the diffraction efficiency. The relation between grating depth and diffraction efficiency was obtained by the coupled-wave theory taking into account the grating characteristics (period, profile and duty-cycle) as well as some other experimental data such as the laser wavelength and the incident angle (Figure S3). The grating period was calculated with high precision from the angle in which the direction of the diffracted order R-1 coincides with that of the incident beam (Figure 2a).

Optical characterization

Absorption spectra of films were obtained using a double-beam Jasco V-650 spectrophotometer and PL measurements were performed with a Jasco FP-6500 spectrofluorimeter. PL quantum yields were measured with a Jasco ISF-834 integrating sphere attached to the fluorimeter.

ASE and DFB laser measurements were performed using a Nd:YAG pulsed laser (10 Hz repetition rate) operating at 355 nm as excitation source. An optical parametric oscillator

(OPO) was used to obtain different excitation wavelengths, starting at 415 nm. For each material the wavelength which maximizes the film absorption, λ_{pump}, was selected (Table 1). The incident pump energy was modified with neutral density filters.

ASE characterization was performed by exciting the sample at normal incidence with a stripe beam (3.5 × 0.5 mm), formed by a cylindrical lens, and the output light was collected from the edge of the film. In the case of the DFB laser characterization the device was excited at a 30º angle with respect to the film normal, with a circular beam, so the spot over the sample is elliptical (minor axis of 1.1 mm) and the emitted light was collected perpendicularly to the film plane. An optical fiber coupled to an Ocean Optics USB2000+ UV-VIS fiber spectrometer with a resolution of 1.3 nm was used in both cases.

ASE and laser thresholds were determined as the lowest pump energy at which these two phenomena occur. Photostability was measured from the decay of the DFB intensity with time, at a pump energy of 10 kW cm^{-2}, and quantified using the half-life parameter, defined as the time at which the DFB intensity decays to half of its initial value.

The studies of possible damage of the active films due to the grating fabrication process were performed on COPV1-t-Bu(Me) (dispersed in PS at 2 wt%; film thickness: 340 nm) and on COPV2 (dispersed in PS at 3 wt%; film thickness: 585 nm). The ABS and PL film spectra and their PLQY and the ASE threshold were measured before and after illumination with the Argon laser (λ = 364 nm) at a pump energy density of 90 mJ/cm^2 (the value used to record the gratings in the holographic process). The same film parameters were recorded before and after exposure to an oxygen plasma for 10 minutes (time used in the development step in the grating fabrication process).

Acknowledgements

The Spanish team acknowledges support from the Spanish Government (MINECO) and the European Community (FEDER) through grant no. MAT2015-66586-R. Japanese authors

thank the financial support from MEXT (JP19H05716 for HT and JP19H0549 for EN). We also thank V. Esteve and I. Garcés for technical assistance.

Received: ((will be filled in by the editorial staff))
Revised: ((will be filled in by the editorial staff))
Published online: ((will be filled in by the editorial staff))

References

[1] S. Chénais, S. Forget, *Polym. Int.* **2012**, *61*, 390.

[2] M. Anni, S. Lattante, *Organic Lasers: Fundamentals, Developments, and Applications*, Pan Stanford Publishing, Singapore, **2018**.

[3] A. J. C. Kuehne, M. C. Gather, *Chem. Rev.* **2016**, *116*, 12823.

[4] Y. Jiang, Y.-Y. Liu, X. Liu, H. Lin, K. Gao, W.-Y. Lai, W. Huang, *Chem. Soc. Rev.* **2020**, *49*, 5885.

[5] A. S. D. Sandanayaka, T. Matsushima, F. Bencheikh, S. Terakawa, W. J. Potscavage, C. Qin, T. Fujihara, K. Goushi, J.-C. Ribierre, C. Adachi, *Appl. Phys. Express* **2019**, *12*, 061010.

[6] E. Heydari, J. Buller, E. Wischerhoff, A. Laschewsky, S. Döring, J. Stumpe, *Adv. Opt. Mater.* **2014**, *2*, 137.

[7] Y. Wang, P. O. Morawska, A. L. Kanibolotsky, P. J. Skabara, G. A. Turnbull, I. D. W. Samuel, *Laser Photon. Rev.* **2013**, *7*, L71.

[8] M. Morales-Vidal, P. G. Boj, J. A. Quintana, J. M. Villalvilla, A. Retolaza, S. Merino, M. A. Díaz-García, *Sensors Actuators B Chem.* **2015**, *220*, 1368.

[9] G. Tsiminis, Y. Wang, A. L. Kanibolotsky, A. R. Inigo, P. J. Skabara, I. D. W. Samuel, G. A. Turnbull, *Adv. Mater.* **2013**, *25*, 2826.

[10] J. R. C. Smirnov, Q. Zhang, R. Wannemacher, L. Wu, S. Casado, R. Xia, I. Rodriguez,

J. Cabanillas-González, *Sci. Rep.* **2016**, *6*, 34565.

[11] N. Tsutsumi, S. Nagi, K. Kinashi, W. Sakai, *Sci. Rep.* **2016**, *6*, 34741.

[12] J. A. Quintana, J. M. Villalvilla, M. Morales-Vidal, P. G. Boj, X. Zhu, N. Ruangsupapichat, H. Tsuji, E. Nakamura, M. A. Díaz-García, *Adv. Opt. Mater.* **2017**, *5*, 1700238.

[13] V. Bonal, J. A. Quintana, J. M. Villalvilla, P. G. Boj, M. A. Díaz-García, *Sci. Rep.* **2019**, *9*, 11159.

[14] T. Virgili, M. Anni, M. L. De Giorgi, R. B. Varillas, B. M. Squeo, M. Pasini, *Molecules* **2020**, *25*, 1.

[15] M. Morales-Vidal, P. G. Boj, J. M. Villalvilla, J. A. Quintana, Q. Yan, N. T. Lin, X. Zhu, N. Ruangsupapichat, J. Casado, H. Tsuji, E. Nakamura, M. A. Díaz-García, *Nat. Commun.* **2015**, *6*, 8458.

[16] D. Okada, S. Azzini, H. Nishioka, A. Ichimura, H. Tsuji, E. Nakamura, F. Sasaki, C. Genet, T. W. Ebbesen, Y. Yamamoto, *Nano Lett.* **2018**, *18*, 4396.

[17] H. Tsuji, E. Nakamura, *Acc. Chem. Res.* **2019**, *52*, 2939.

[18] M. Morales-Vidal, J. A. Quintana, J. M. Villalvilla, P. G. Boj, H. Nishioka, H. Tsuji, E. Nakamura, G. L. Whitworth, G. A. Turnbull, I. D. W. Samuel, M. A. Díaz-García, *Adv. Opt. Mater.* **2018**, *6*, 1800069.

[19] V. Bonal, M. Morales-Vidal, P. G. Boj, J. M. Villalvilla, J. A. Quintana, N. Lin, S. Watanabe, H. Tsuji, E. Nakamura, M. A. Díaz-García, *Bull. Chem. Soc. Jpn.* **2020**, *93*, 751.

[20] K. Kazlauskas, G. Kreiza, O. Bobrovas, O. Adomėnienė, P. Adomėnas, V. Jankauskas, S. Juršėnas, *Appl. Phys. Lett.* **2015**, *107*, 043301.

[21] V. Bonal, J. A. Quintana, R. Muñoz-Mármol, J. M. Villalvilla, P. G. Boj, M. A. Díaz-García, *Thin Solid Films* **2019**, *692*, 137580.

[22] GSolver, www.gsolver.com.

[23] M. G. Ramírez, J. M. Villalvilla, J. A. Quintana, P. G. Boj, M. A. Díaz-García, M. G. Ramirez, P. G. Boj, V. Navarro-Fuster, I. Vragovic, J. M. Villalvilla, I. Alonso, V. Trabadelo, S. Merino, M. A. Díaz-García, *Opt. Mater. Express* **2014**, *4*, 733.

[24] J. M. Villalvilla, J. A. Vallés-Abarca, J. A. Quintana, J. Crespo, *J. Vac. Sci. Technol. B Microelectron. Nanom. Struct.* **1999**, *17*, 1085.

[25] R. Kazarinov, C. Henry, *IEEE J. Quantum Electron.* **1985**, *21*, 144.

[26] H. J. Luo, P. S. Zory, *IEEE Photonics Technol. Lett.* **1990**, *2*, 614.

[27] H. J. Luo, P. S. Zory, *IEEE J. Quantum Electron.* **1994**, *30*, 10.

[28] C. Sigler, X. Wang, L. J. Mawst, P. S. Zory, *IEEE J. Quantum Electron.* **2018**, *54*, 1.

[29] P. M. Burrezo, N.-T. Lin, K. Nakabayashi, S. Ohkoshi, E. M. Calzado, P. G. Boj, M. A. Díaz García, C. Franco, C. Rovira, J. Veciana, M. Moos, C. Lambert, J. T. López Navarrete, H. Tsuji, E. Nakamura, J. Casado, *Angew. Chemie Int. Ed.* **2017**, *56*, 2898.

[30] J. Sukegawa, H. Tsuji, E. Nakamura, *Chem. Lett.* **2014**, *43*, 699.

[31] Q. Yan, Y. Guo, A. Ichimura, H. Tsuji, E. Nakamura, *J. Am. Chem. Soc.* **2016**, *138*, 10897.

[32] S. Klinkhammer, X. Liu, K. Huska, Y. Shen, S. Vanderheiden, S. Valouch, C. Vannahme, S. Bräse, T. Mappes, U. Lemmer, *Opt. Express* **2012**, *20*, 6357.

[33] K. Zhang, Q. Zhang, H. Zhang, J. Shen, Q. Niu, R. Xia, *Macromol. Chem. Phys.* **2018**, *219*, 1700527.

[34] R. Muñoz-Mármol, N. Zink-Lorre, J. M. Villalvilla, P. G. Boj, J. A. Quintana, C. Vázquez, A. Anderson, M. J. Gordon, A. Sastre-Santos, F. Fernández-Lázaro, M. A. Díaz-García, *J. Phys. Chem. C* **2018**, *122*, 24896.

[35] H. Kogelnik, C. V. Shank, *J. Appl. Phys.* **1972**, *43*, 2327.

[36] V. Navarro-Fuster, I. Vragovic, E. M. Calzado, P. G. Boj, J. A. Quintana, J. M. Villalvilla, A. Retolaza, A. Juarros, D. Otaduy, S. Merino, M. A. Díaz-García, *J. Appl. Phys.* **2012**, *112*, 043104.

[37] V. T. N. Mai, A. Shukla, A. M. C. Senevirathne, I. Allison, H. Lim, R. J. Lepage, S. K. M. McGregor, M. Wood, T. Matsushima, E. G. Moore, E. H. Krenske, A. S. D. Sandanayaka, C. Adachi, E. B. Namdas, S.-C. Lo, *Adv. Opt. Mater.* **2020**, 2001234.

[38] M. Fang, J. Huang, S. J. Chang, Y. Jiang, W. Y. Lai, W. Huang, *J. Mater. Chem. C* **2017**, *5*, 5797.

[39] G. Tsiminis, N. A. Montgomery, A. L. Kanibolotsky, A. Ruseckas, I. F. Perepichka, P. J. Skabara, G. A. Turnbull, I. D. W. Samuel, *Semicond. Sci. Technol.* **2012**, *27*, 094005.

[40] B. K. Yap, R. Xia, M. Campoy-Quiles, P. N. Stavrinou, D. D. C. Bradley, *Nat. Mater.* **2008**, *7*, 376.

[41] W. Huang, S. Shen, D. Pu, G. Wei, Y. Ye, C. Peng, L. Chen, *J. Phys. D. Appl. Phys.* **2015**, *48*, 495105.

[42] T. Spehr, A. Siebert, T. Fuhrmann-Lieker, J. Salbeck, T. Rabe, T. Riedl, H. H. Johannes, W. Kowalsky, J. Wang, T. Weimann, P. Hinze, *Appl. Phys. Lett.* **2005**, *87*, 161103.

[43] E. M. Calzado, M. G. Ramírez, P. G. Boj, M. A. Díaz-García, *Appl. Opt.* **2012**, *51*, 3287.

[44] M. Anni, A. Perulli, G. Monti, *J. Appl. Phys.* **2012**, *111*, 093109.

a

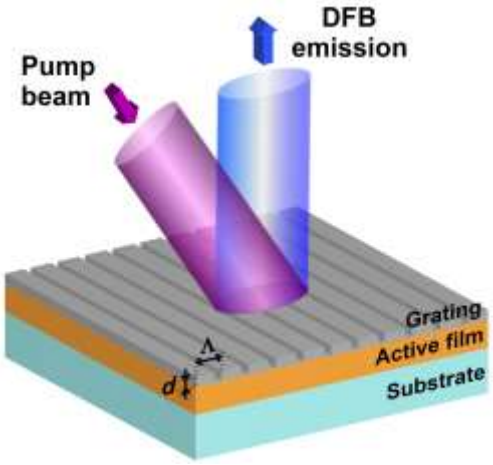

b

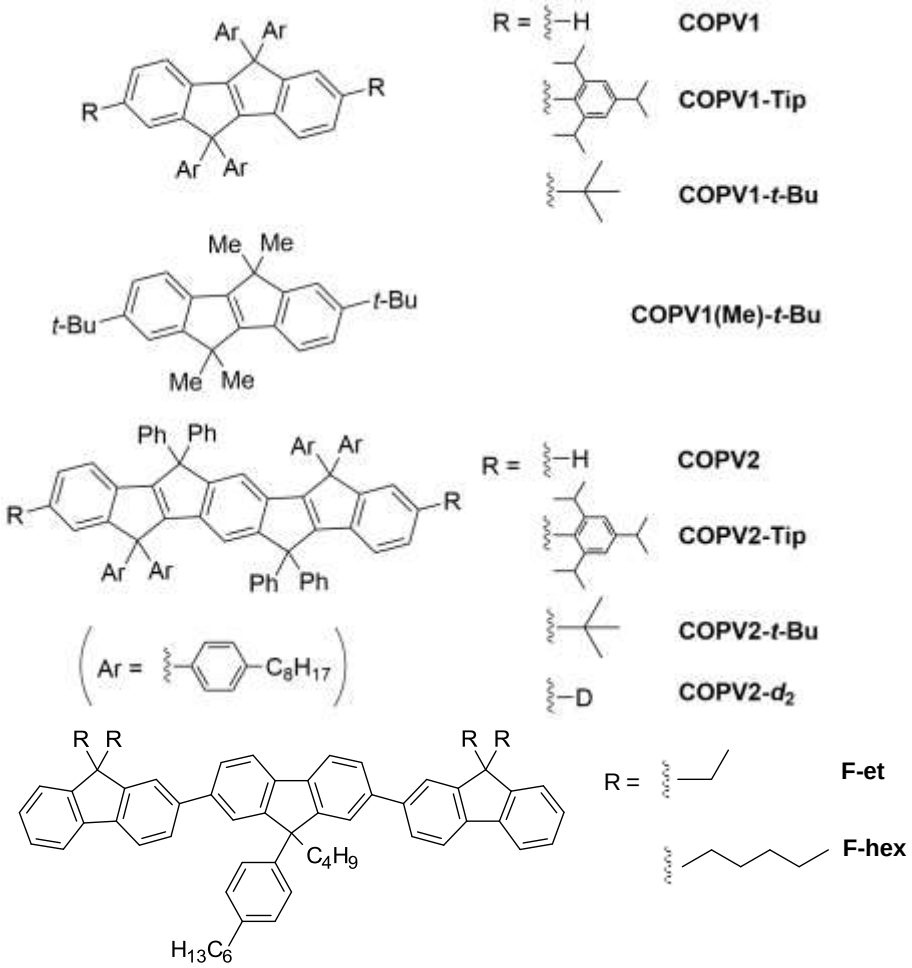

Figure 1. DFB architecture and active materials. (a) Scheme of the DFB device architecture, including and pumping and collection geometry (Λ: grating period; *d*: grating depth) (b) Chemical structures of the COPV*n* (with *n* = 1,2) compounds and the terfluorene compounds F-et and F-hex.

a

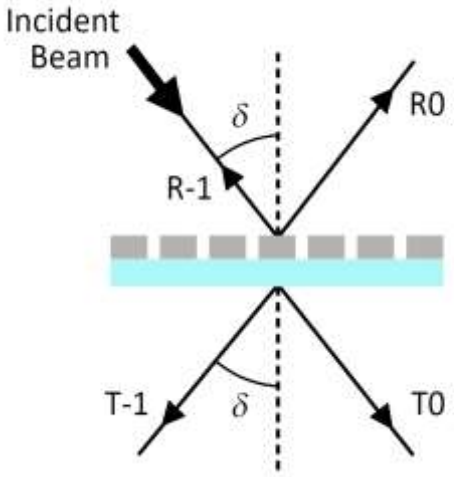
Incident
Beam
δ
R0
R-1
T-1
δ
T0

b

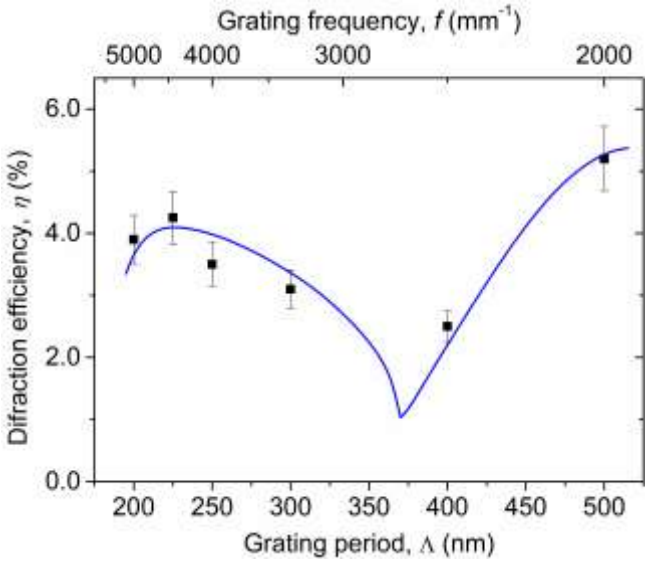
Grating frequency, f (mm-1)
5000
4000
3000
2000
6.0
4.0
2.0
0.0
Diffraction efficiency, η (%)
200
250
300
350
400
450
500
Grating period, Λ (nm)

c

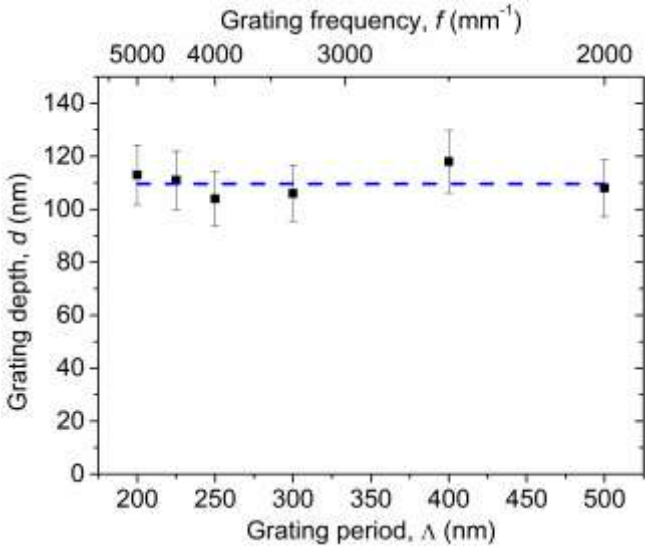
Grating frequency, f (mm-1)
5000
4000
3000
2000
140
120
100
80
60
40
20
0
Grating depth, d (nm)
200
250
300
350
400
450
500
Grating period, Λ (nm)

Figure 2. Resolution analysis of the resonator fabrication process. (a) Scheme of the diffraction efficiency (η) measurement conditions: R and T account for the reflected and transmitted beams, respectively; the numbers for the order of diffraction; and δ for the incident angle. η was measured following a holographic criterion: the δ value for each grating (with period Λ and frequency *f*) was the one used to record the grating; (b) η of the first order transmitted beam as a function of Λ and *f* (bottom and top axis, respectively). Full squares are experimental data and the full line corresponds to simulations; (c) Grating depth, *d*, calculated from η data shown in b), versus Λ and *f* (bottom and top axis, respectively). Simulations have been done with the Gsolver software program (see details in the supporting information, Figures S2 and S3).

a

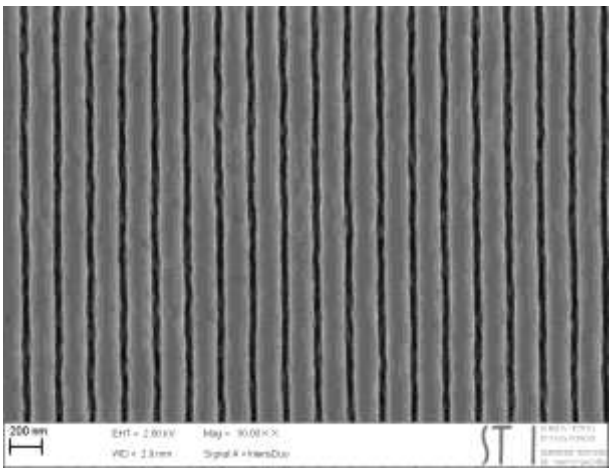
200 nm

b

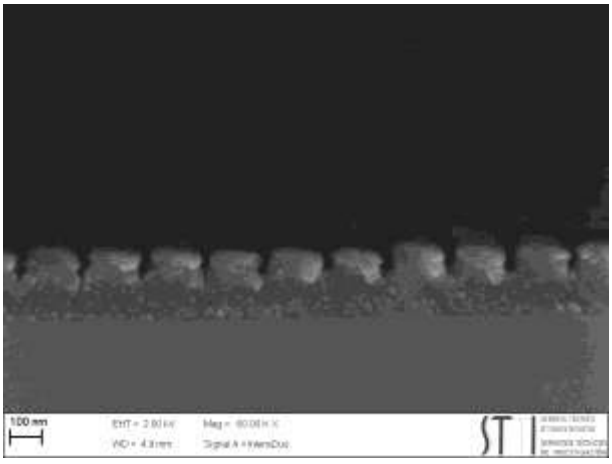
100 nm

c

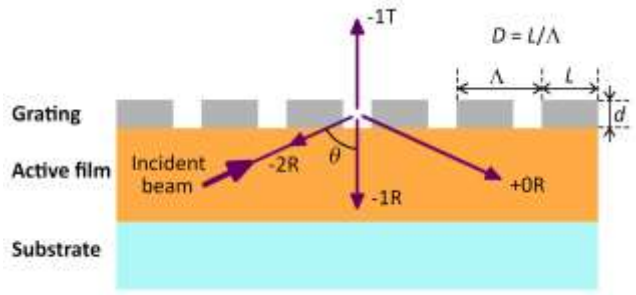
-1T
D = L/Λ
Λ
L
d
Grating
Active film
Substrate
Incident beam
-2R
θ
-1R
+0R

d

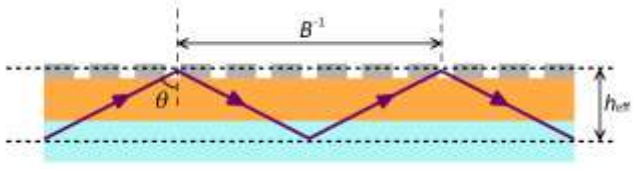
B⁻¹
θ
h

e

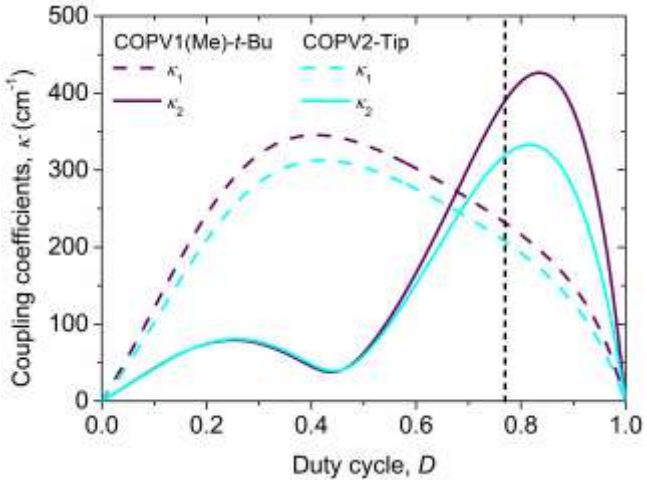

Figure 3. Effect of the duty cycle. (a) Top and (b) lateral FESEM images of a DCG grating with Λ = 200 nm and d = 110 nm; (c) Scheme of a top-layer resonator DFB laser with a square grating profile (D: duty cycle). The various diffracted beams are indicated in an optics-ray approximation with arrows: first order transmitted (-1T) and reflected (-1R); second-order reflected (-2R); zero-order reflected (+0R); (d) Definition of waveguide parameters needed to calculate the bounce rates and the coupling coefficients (equations 3 and 4); (e) Simulations of coupling coefficients κ_1 (dashed lines) and κ_2 (solid lines) versus duty-cycle, D, for top-layer resonator DFB lasers with grating periods of 235 nm and 300 nm based on COPV1(Me)-*t*-Bu (blue lines) and COPV2-Tip (purple lines), respectively. The vertical black short dashed line indicates the experimental D value of the devices used for the simulation.

a

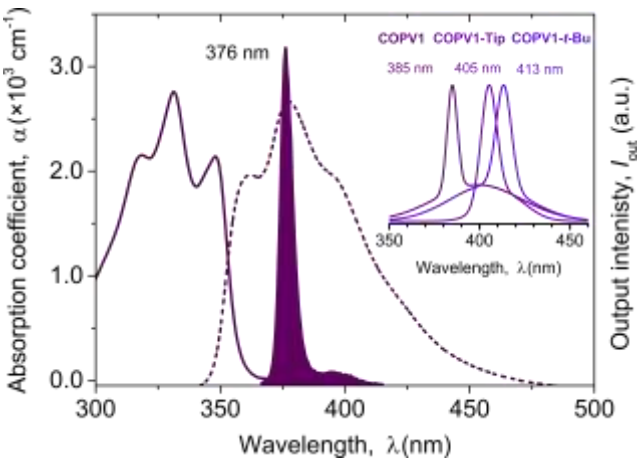
376 nm
COPV1 COPV1-Tip COPV1-t-Bu
385 nm 405 nm 413 nm
Absorption coefficient, α (×10³ cm⁻¹)
Output intenisty, I_out (a.u.)
Wavelength, λ(nm)

b

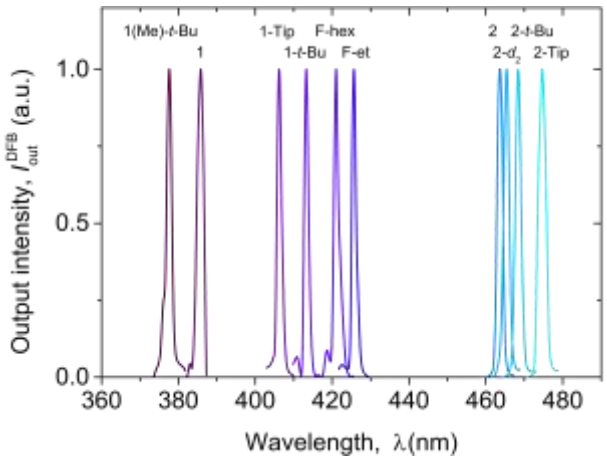
1(Me)-t-Bu
1
1-Tip
1-t-Bu
F-hex
F-et
2
2-t-Bu
2-d2
2-Tip
Output intensity, I_out^DFB (a.u.)
Wavelength, λ(nm)

c

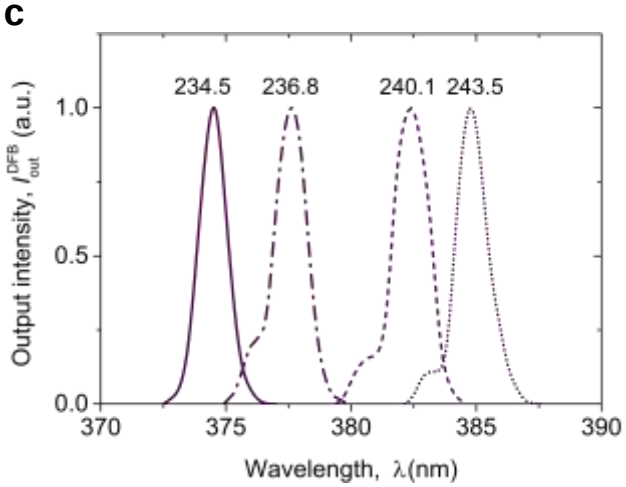
234.5
236.8
240.1
243.5
Output intensity, I_out^DFB (a.u.)
Wavelength, λ(nm)

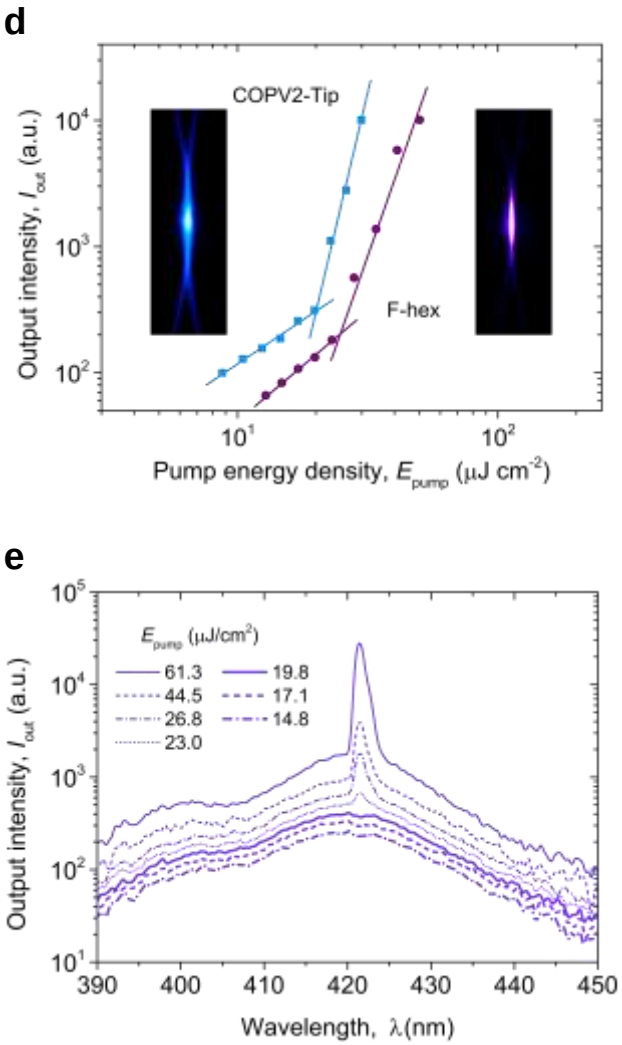

Figure 4. Laser properties. (a) Optical properties of PS films doped with COPV1(Me)-*t*-Bu: Absorption coefficient, α (solid line, left axis), photoluminescence intensity (dashed line, right axis), and amplified spontaneous emission, ASE, intensity (filled area, right axis), versus wavelength, λ. The inset shows the ASE spectra of the other COPV1 compounds used (COPV1, COPV1-Tip and COPV1-*t*-Bu); (b) DFB laser emission of ten devices, each based on a different compound, covering a wavelength emission range between 375 and 475 nm; (c) DFB spectra of COPV1(Me)-*t*-Bu-based devices with different grating periods (values in nm shown next to each peak); (d) Output intensity as a function of the pump energy density (E_{pump}) for the lasers based on COPV2-Tip (blue) and F-hex (purple). Full lines are guides to the eye. The inset shows images of the total light emitted by those same devices; (e) Evolution of the laser spectrum with E_{pump} for the device based on F-hex

Table 1. Geometrical and performance parameters for a selection of prepared DFB lasers. Parameters of top-layer DFB lasers based on active films of ten different organic compounds dispersed in polystyrene. The resonator is a dichromated gelatine (DCG) relief grating with a depth d = 110 nm.

Active material	Dye conc.[a] [wt. % in PS]	Dye conc.[a] [moles dye/g PS ×10^{-7}]	PLQY[b] [%]	λ_p[c] [nm]	$\alpha(\lambda_p)$[e] [×10^3 cm^{-1}]	t_p[f] [ns]	λ_{ASE}[g] [nm]	Λ[i] [nm]	λ_{DFB}[j] [nm]	$E_{th\text{-}DFB}$[k] [μJ cm^{-2}]	$I_{th\text{-}DFB}$[k] [kW cm^{-2}]	$\tau_{1/2}^{DFB}$[l] [pump pulses]
COPV1	5.0	550	100±7	355	1.9	10	385.2	244	385.7	2000	200	-
COPV1-Tip	6.9	550	96±5	355	3.0	10	404.7	256	406.2	900	90	-
COPV1-*t*-Bu	5.6	550	100±7	355	2.4	10	413.4	263	413.3	1200	120	-
COPV1(Me)-*t*-Bu	2.0	550	100±6	355	0.8	10	376.0	237	377.6	1000	100	-
F-hex	10	1062	94±3	355	7.6	10	419.5	266	421.5	25	2.5	1.2×10^4
F-et	50	6083	89±2	355	41	10	422.1	258	425.2	25	2.5	-
COPV2	3.0	223	85±7	423	2.5	3.8	462.7	293	463.6	20	5.5	2.1×10^4
COPV2-Tip	3.8	223	90±7	430	3.1	3.8	473.8	300	474.7	20	5.5	7.7×10^4
COPV2-*t*-Bu	3.7	223	82±7	427	2.8	3.8	469.0	297	468.4	30	8.0	-
COPV2-d_2	3.0	223	86±7	423	2.6	3.8	465.2	299	465.4	30	8.0	-

[a] Error ~0.1%
[b] Photoluminescence quantum yield
[c] Pump wavelength
[e] Absorption coefficient at λ_{pump} (error ~2%)
[f] Pump pulse width at λ_{pump}
[g] ASE wavelength (error is ± 0.5 nm)
[i] Grating period (error ~0.5%)
[j] DFB wavelength (error is ± 0.5 nm)
[k] DFB threshold (error ~10%), determined from Fig. 4d, expressed as energy density, $E_{th\text{-}DFB}$, or power density, $I_{th\text{-}DFB} = E_{th\text{-}DFB} / t_p$ (t_p is the pump pulse width, values in Table 1)
[l] DFB operational lifetime, characterized by the photostability half-life $\tau_{1/2}^{DFB}$ (measured in air under a pump intensity of 10 kW cm^{-2} at 10 Hz (error ~10%).

The table of contents entry should be 50–60 words long, and the first phrase should be bold. The entry should be written in the present tense and impersonal style. The text should be different from the abstract text.

All-solution processed organic distributed feedback lasers, based on top-layer polymeric resonators, emitting between 375 and 475 nm are reported. Active films are prepared with ten different organic dyes dispersed in polystyrene, including a new compound with deep-blue emission, COPV1(Me)-*t*-Bu, along with its synthesis and optical properties. The top-layer resonator configuration used shows high performance in all cases.

Keyword
organic lasers, solution-processed, distributed feedback lasers, polymeric resonators

*Victor Bonal, Jose M. Villalvilla, Jose A. Quintana, Pedro G. Boj, Naiti Lin, Shoya Watanabe, Karolis Kazlauskas, Ona Adomeniene, Saulius Jursenas, Hayato Tsuji, Eiichi Nakamura, María A. Díaz-García**

Title
Blue and deep-blue emitting organic lasers with top-layer distributed feedback resonators

ToC figure ((Please choose one size: 55 mm broad × 50 mm high **or** 110 mm broad × 20 mm high. Please do not use any other dimensions))